Supporting Information Appendix

Autonomous Treatment of Bacterial Infections *In Vivo* Using Antimicrobial Micro- and Nanomotors

Xavier Arqué[1,‡], Marcelo D. T. Torres[2-4,‡], Tania Patiño[1,5], Andreia Boaro[2-4], Samuel Sánchez[1,6,], Cesar de la Fuente-Nunez[2-4,*]*

SUPPORTION INFORMATION FIGURES

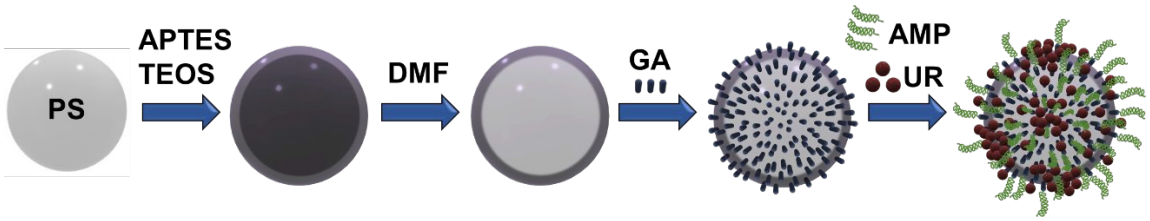

Figure S1. Schematic of the synthesis of urease micromotors. Polystyrene (PS) microbeads (D = 2 μm) were used to grow silica on top starting off 3-aminopropyltriethoxysilane (APTES) and tetraethylorthosilicate (TEOS) precursors. Dimethylformamide is used to dissolve the PS core and keep the silica shell where glutaraldehyde (GA) linker is used to attach urease (UR) and the antimicrobial peptide (AMP) payload.

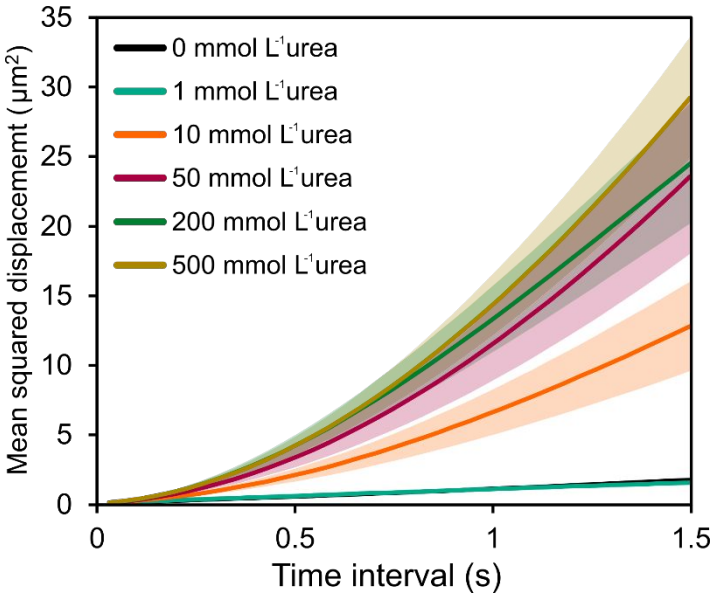

Figure S2. Mean square displacement (MSD) of urea micromotors for urea concentration. MSD growth extracted from X and Y position of micromotors recorded through microscopy, representing the average area explored for each time interval and under different concentrations of urea (substrate). All results are shown as the mean ± standard error of the mean.

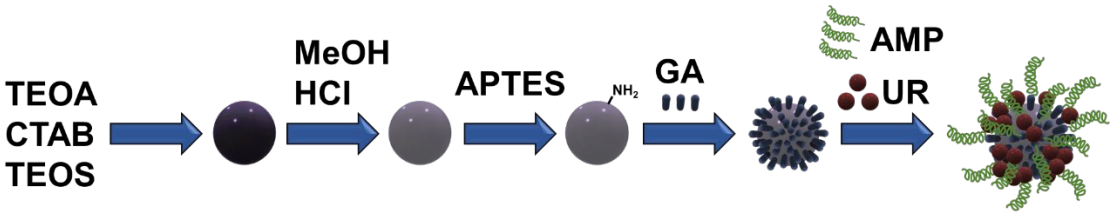

Figure S3. Schematic of the synthesis of urease nanomotors. Triethanolamine (TEOA) and hexadecyltrimethylammonium bromide (CTAB) are mixed to generate silica nanoparticles by dropwise addition of tetraethylorthosilicate (TEOS). After, the CTAB is removed by addition of methanol (MeOH) and hydrochloric acid (HCl) and the mesopores are formed. To functionalize the silica nanoparticles the surface is modified with amino groups adding 3-aminopropyltriethoxysilane (APTES). The glutaraldehyde (GA) linker is used to attach urease (UR) and the antimicrobial peptide (AMP) payload.

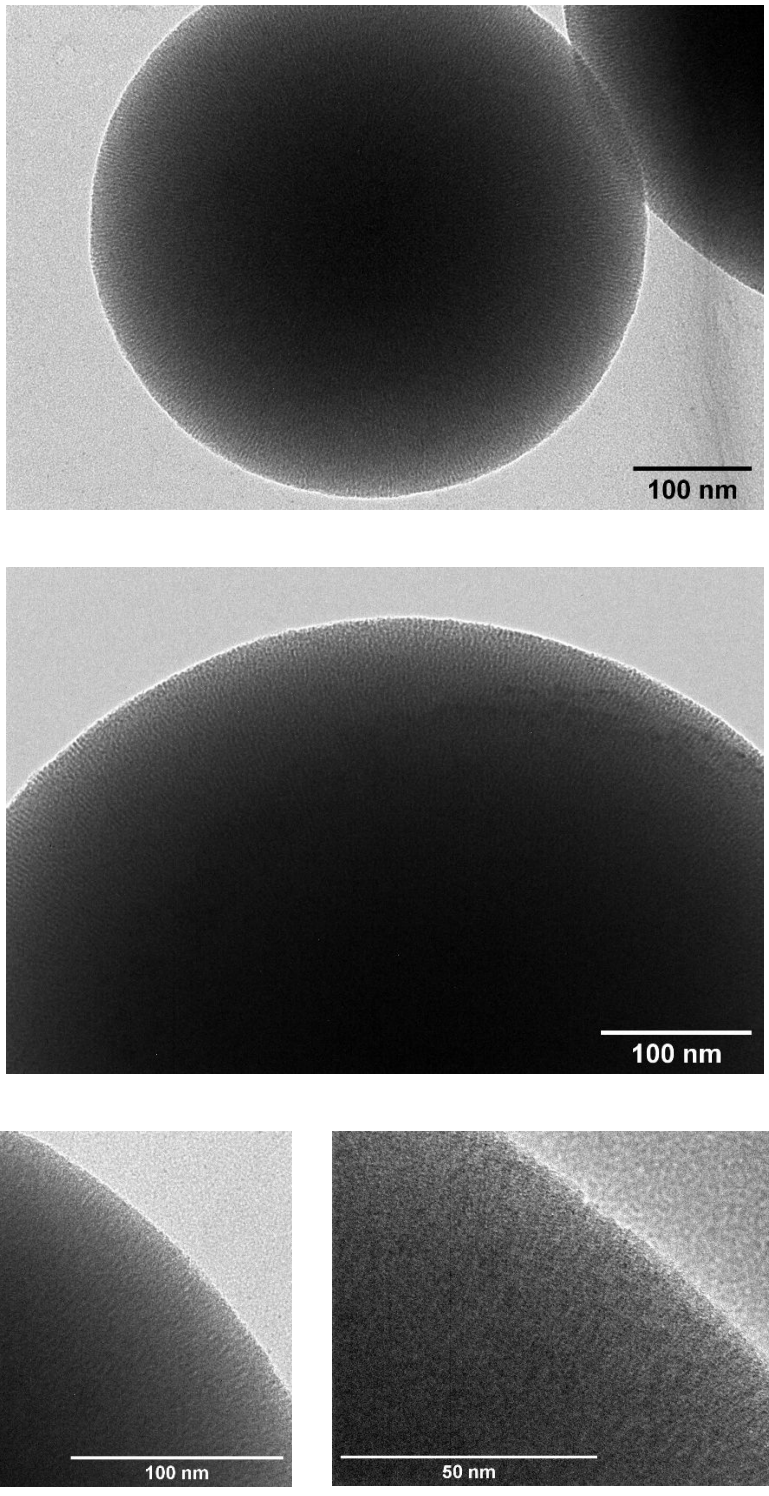

Figure S4. TEM micrograph of silica nanoparticles (MSNP). Micrographs of increasing magnification showing the radial mesoporosity channels inside the silica structure after the removal of CTAB, clearly visible specially in the outer area of the sphere.

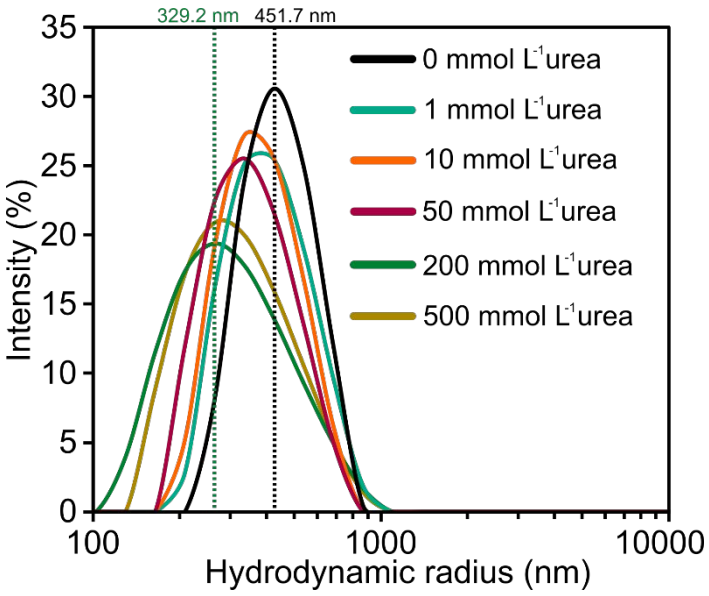

Figure S5. Hydrodynamic radius of urease nanomotors for different concentrations of urea. Representative hydrodynamic radii dispersion of urease nanomotors obtained through Dynamic Light Scattering (DLS) by measuring the diffusion of the particles and applying the Stokes−Einstein equation (see Methods section for details) to derive the radius for each urea concentration used.

Table S1. Antimicrobial activity of bioactive micro- and nanomotors functionalized with antimicrobial peptides.

System	Minimial Inhibitory Activity (μg mL^{-1})				
	A. baumannii AB177	*E. coli* ATCC11775	*K. pneumoniae* ATCC13883	*P. aeruginosa* PAO1	*S. aureus* ATCC12600
HSMP-Urease	62.5	62.5	125	31.2	500
HSMP-Urease-LL-37	7.8	7.8	31.2	7.8	31.2
HSMP-Urease-K7-Pol	7.8	7.8	31.2	7.8	31.2
MSNP-Urease	62.5	125	>500	62.5	>500
MSNP-Urease-LL-37	15.6	7.8	31.2	7.8	31.2
MSNP-Urease-K7-Pol	15.6	15.6	31.2	15.6	31.2
LL-37	1	0.4	2	4	4
K7-Pol	0.2	0.1	0.4	0.4	0.4
Polymyxin B	5.4	5.4	44.3	5.4	88.7

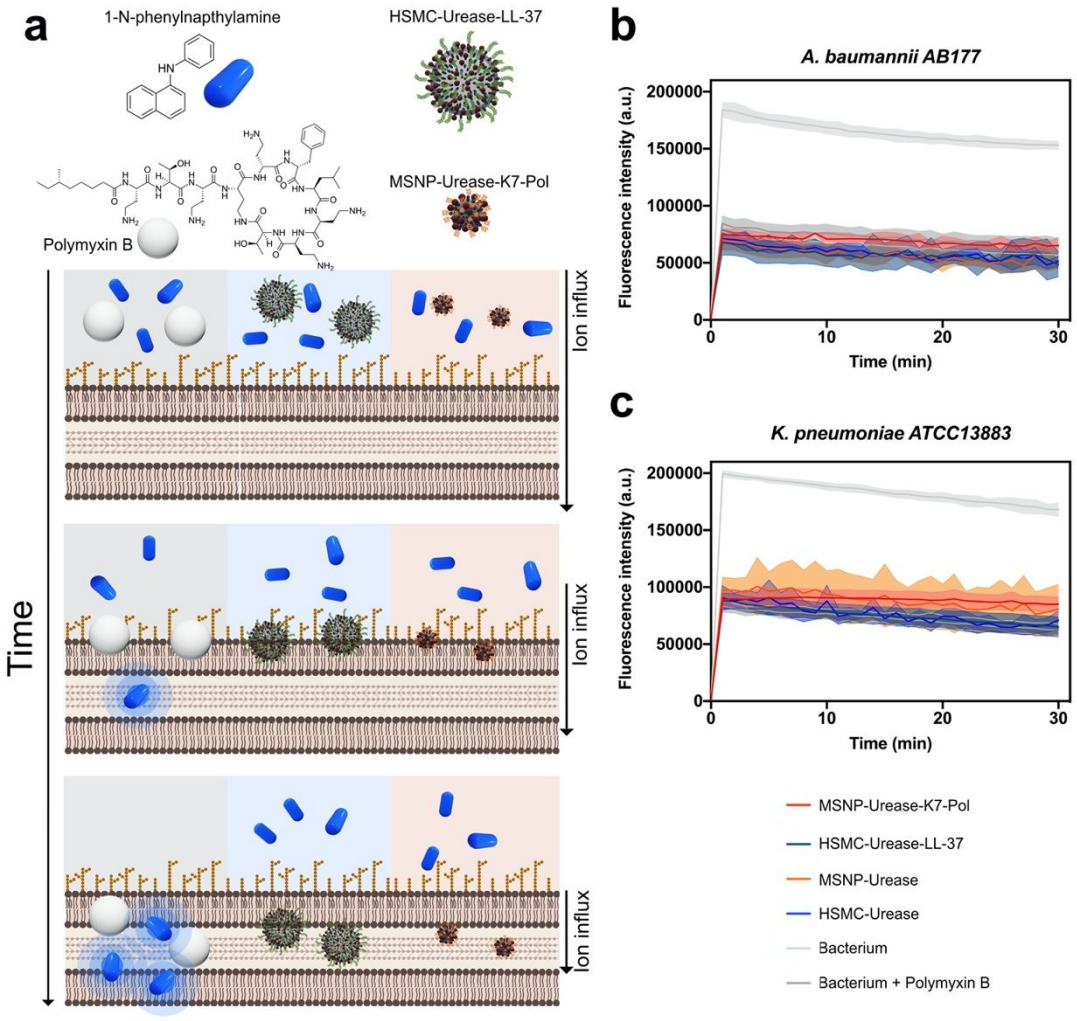

Figure S6. Membrane permeabilization experiments with urease micro- and nanomotors functionalized with peptides. (a) Motors do not permeabilize bacterial membranes at their MIC concentration against **(b)** *A. baumannii* AB177 and **(c)** *K. pneumoniae* ATCC13883. The permeabilizing antimicrobial polymyxin B was used as a positive control for permeabilization of the bacterial membranes. This figure was created with BioRender.com.

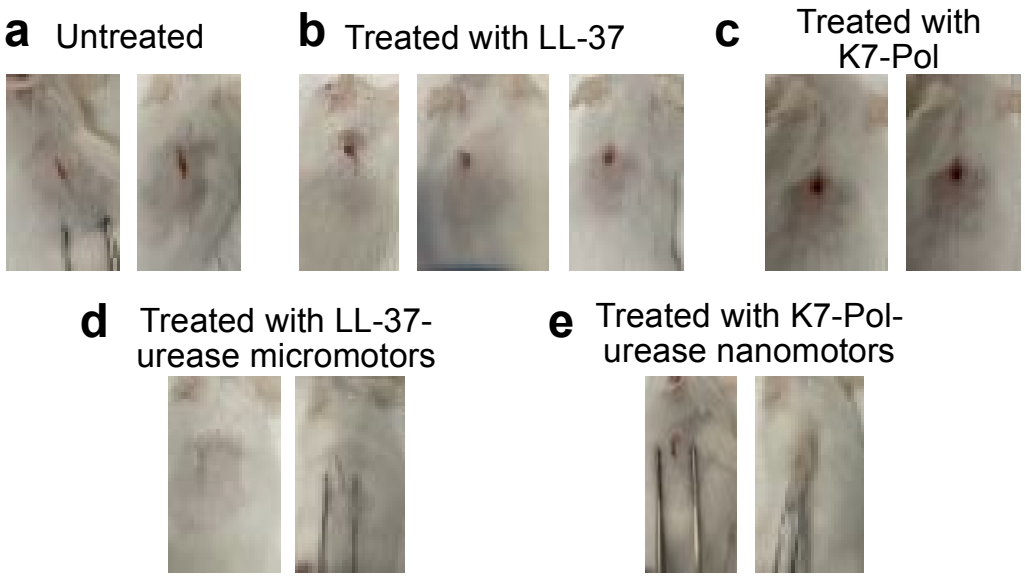

Figure S7. Images of the infection site on the back of mice used for the *in vivo* anti-infective model. The images show (a) an untreated infection colonized by bacteria, (b) treatment with LL-37 that leads to partial wound healing, (c) treatment with K7-Pol that resolve the infection only at the administration site (bottom part of the wound), (d) treatment with the antimicrobial peptide payloads delivered by LL-37-urease micromotors that clear the whole extent of the wound and promote complete wound healing, and (e) treatment with the antimicrobial peptide payloads delivered by K7-Pol-urease nanomotors that resolve the infection but do not promote full wound healing.

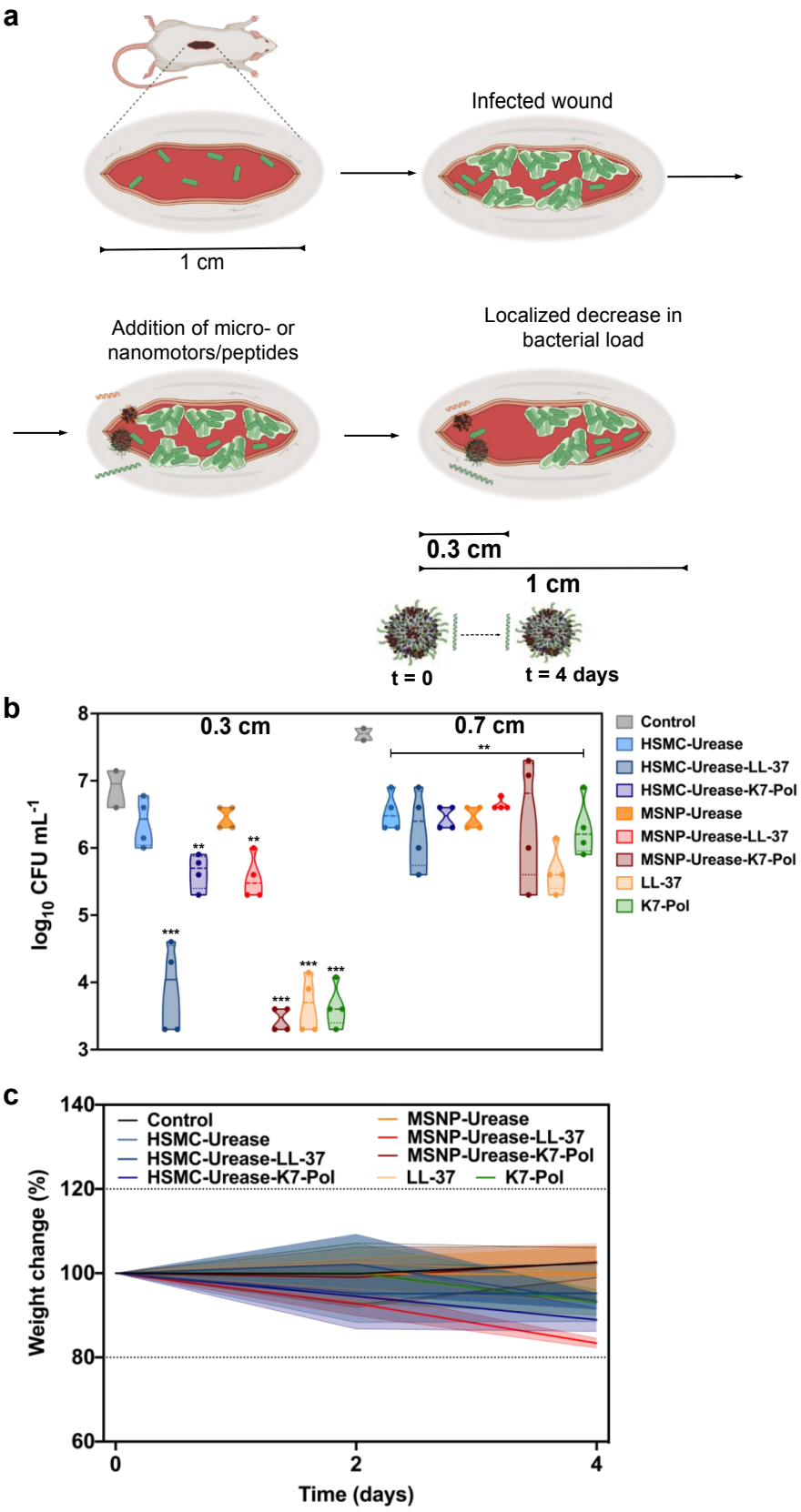

Figure S8. Anti-infective activity of the antimicrobial motors *in vivo* in the absence of urea. (a) Schematic representation of the wound site infected in the absence of urea

and treated either with micro- and nanomotors or peptides free in solution. Antimicrobial micro- and nanomotors and peptides by themselves only exhibited antimicrobial activity within the area they were administered (within 0.3 cm of the administration site) and did not clear the infection at a distance (1 cm). **(b)** Four days post-infection, 1 cm^2 of the infected area was excised and peptide-functionalized micro- and nanomotors and peptides alone decreased bacterial counts only in the extremity where they were administered (light yellow background) as revealed by similar bacterial counts detected in areas at a distance from the administration site (dark yellow background) and those of untreated control groups. **(c)** Mouse weight was monitored throughout the experiments, serving to monitor potential of all the treated and untreated groups (20% variation was used as threshold). Four animals were used per group. This figure was created with BioRender.com.

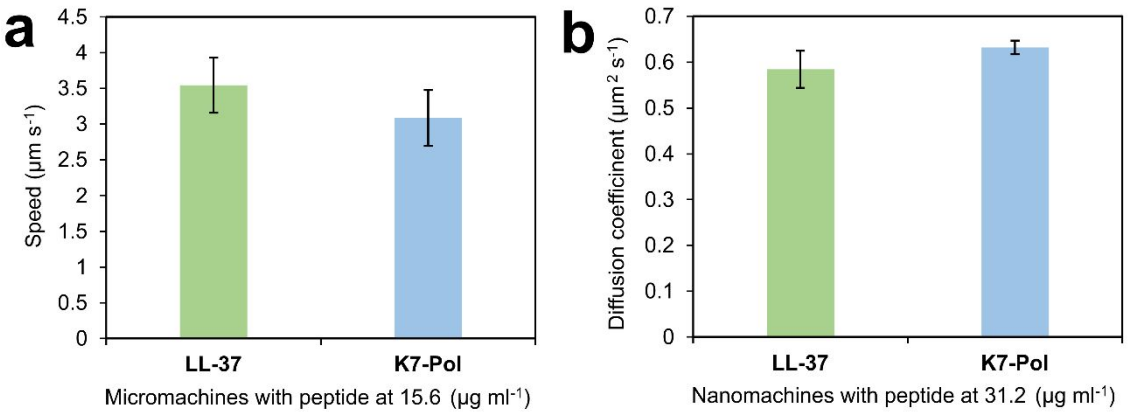

Figure S9. Comparison of active motion of micro- and nanomotors with different antimicrobial peptides attached. (a) Average speed of urease micromotors and **(b)** average diffusion coefficient of urease nanomotors modified with K7-Pol and LL-37 at the concentration used *in vivo* (15.6 µg mL^{-1} for micromotors and 31.2 µg mL^{-1} for nanomotors). No significant differences in motion were found between the peptides when anchored at the same concentration to the micro- and nanomotors.